Applied Catalysis B: Environmental 89 (2009) 229–238

Contents lists available at ScienceDirect

Applied Catalysis B: Environmental

journal homepage: www.elsevier.com/locate/apcatb

Microkinetic modeling for hydrocarbon (HC)-based selective catalytic reduction (SCR) of NO_x on a silver-based catalyst

Ashish B. Mhadeshwar [a], Benjamin H. Winkler [a], Boris Eiteneer [b], Dan Hancu [a,*]

[a] GE Global Research, 1 Research Circle, Niskayuna, NY 12309-1027, United States
[b] GE Global Research, 18A Mason Road, Irvine, CA 92618-2706, United States

ARTICLE INFO

Article history:
Received 28 July 2008
Received in revised form 20 January 2009
Accepted 13 February 2009
Available online 25 February 2009

Keywords:
NO_x
SCR
Microkinetic model
Ethanol
Hydrocarbon
Silver

ABSTRACT

Modeling of aftertreatment systems for NO_x abatement from fuel combustion is a critical step in catalyst design. Selective catalytic reduction (SCR) is a key component in the overall aftertreatment system. In this paper, we focus on developing a detailed elementary reaction mechanism for hydrocarbon (HC)-based SCR on a silver-impregnated monolith catalyst. Rather than developing a single rate expression based on power-law fitting or Langmuir–Hinshelwood kinetics, a detailed microkinetic modeling approach is utilized to capture the essential physics of this problem. Even though the system is complicated, with more than 10 reductants along with some promoting or inhibiting effects of other species, a hierarchical approach for mechanism development is used to retain the simplicity of the mechanism in terms of computational implementation. The HC-SCR mechanism is shown to capture experimental data for all reductants, in most cases, quantitatively.

1. Introduction

Selective catalytic reduction (SCR) is currently considered one of the most promising methods to reduce NO_x under excess oxygen conditions. Significant research work has been published over the last decade, focusing on SCR mechanism investigation and catalyst discovery, e.g., see [1–12] and references therein. Even though urea-SCR has been a popular research area from industrial perspective, hydrocarbon (HC)-based SCR has also received a significant attention lately. Burch and Murzin research groups deserve special mention for their pioneering research in investigating the HC-SCR mechanism in detail [5,8,13–26]. Power-law [20] and Langmuir–Hinshelwood [18] models have also been developed for HC-SCR. However, a detailed elementary microkinetic mechanism has not yet been developed for this complicated chemistry. Microkinetic modeling has various advantages over power-law fits and Langmuir–Hinshelwood expressions, e.g., it is valid over a wide range of operating conditions, it does not require any assumptions regarding the rate-determining step or partial equilibrium, and the rate parameters are generally extracted from experiments or calculated using theoretical techniques rather than data fitting [27]. Since the inception of microkinetic modeling [28], Vlachos, Deutschmann, and Schmidt research groups have made significant advances in applications of microkinetic modeling for various catalytic systems [29–35]. Vlachos research group has also demonstrated novel ideas such as thermodynamic consistency [27] and hierarchical mechanism development [36].

In this work, we employ similar concepts to develop a novel microkinetic mechanism for HC-SCR of NO_x on an Ag-based catalyst. The choice of catalyst is driven by the fact that Ag/Al_2O_3 has been shown to have high activity for HC-SCR of NO_x compared to other catalysts [37] and Al_2O_3 [38]. First, we explain the details of the lab-scale experimental setup. Then, we focus on the development of the HC-SCR microkinetic mechanism, including parameter estimation and tuning based on our lab-scale experimental data. Literature insights regarding HC-SCR chemistry and reaction pathways are taken into account while developing the mechanism. Next, performance of this mechanism is discussed along with various parametric effects. Finally, we also mention the limitations and assumptions of this kinetic mechanism. For the first time, a comprehensive reaction mechanism has been developed for the HC-SCR chemistry. This mechanism can have wide applications for integrated aftertreatment systems simulations.

2. Experimental

Overall schematic of the lab-scale experimental setup is shown in Fig. 1. The catalyst is installed in a quartz-tube reactor located inside a furnace. Temperature, pressure, space velocity over the

* Corresponding author. Tel.: +1 518 387 5011; fax: +1 518 387 7611.
E-mail address: hancuda@crd.ge.com (D. Hancu).

0926-3373/$ – see front matter © 2009 Elsevier B.V. All rights reserved.
doi:10.1016/j.apcatb.2009.02.012

catalyst, and gas composition at the inlet of the reactor are controlled. The reactor is fully automated and experimental test matrix can be run over extended period of time (days or weeks). Extractive gas analysis is used for the measurement of NO, NO_2 (chemiluminescence detector), CO, CO_2 (IR detector), and SO_2 (UV–vis detector). A diesel oxidation Pt/Al_2O_3 catalyst (DOC) bed located upstream of the sampling point can be either flown through or by-passed. NO_x conversion is defined as follows:

$$NO_x \text{ conversion } (\%) = 100 \times \left(1 - \frac{[NO_x]_{outlet}}{[NO_x]_{inlet}}\right)$$

HC-SCR catalysts were prepared in the form of washcoated monoliths by metal impregnation onto SBA 200 γ-alumina, washcoated on cordierite. These supported catalysts are 230 cpsi (cells per square inch) monoliths. The washcoat loading is ∼150 g/L (grams of washcoated alumina per liter of monolith), washcoat thickness is ∼4 mil, washcoat profile is axially uniform and the catalyst contains 2% Ag.

Catalysts were tested under experimental conditions listed in Table 1. The catalyst length of the HC-SCR was 2 cm. The corresponding space velocity (for a 5.35 SLPM volumetric flowrate) was ∼61,000 h^{-1}. The monolith catalyst was wrapped with a thin layer (<1 mm) of Interam 100 (3M) and loaded into a quartz tube with an inner diameter of 1.9 cm and length of 35 in. The monolith was placed at least 24 in. from the inlet of the quartz tube to allow for preheating of the feed gas. A plug of 0.5 g of quartz wool was placed on either side of the monolith. From our experience in SCR testing, it is known that CO_2 in feed does not promote or inhibit the NO_x conversion. Therefore, it was not included in the testing for simplicity. On the other hand, we have included water in the testing because water has been shown to have a significant effect on NO_x conversion. For example, water can have promoting effect on C_3H_6-SCR and inhibiting effect on ethanol-SCR [39].

Liquid reductants were pumped by an HPLC pump, and diluted and vaporized at 200–300 °C with nitrogen before being injected in the reactor. Gaseous reductants were delivered using the Environics gas blending system with balance nitrogen. The amount of reductant injected was quantified by deep oxidation on Pt/Al_2O_3 catalyst at 450 °C (space velocity below 20,000 h^{-1}) followed by the measurement of CO_2 concentration in the gas stream. The assumption that full catalytic combustion of the reductants took place was validated by the fact that very low CO concentrations were measured. Also, deep oxidation of reductants provided the C_1 (ppm of molecular carbon) equivalent number (equal to CO_2 concentration in ppm), which allows for the computation of the C_1:NO_x ratio.

Table 1
Lab-scale experimental conditions.

Variable	Unit	
Temperature	°C	305, 375, 435
[NO]	ppm	475, 600, 689
[H_2]	ppm	0 and 1000
Space velocity	h^{-1}	61,000
C_1:NO_x ratio		5:1
[Water]	mol%	7
[SO_2]	ppm	0
[CO_2]	ppm	0
[CO]	ppm	250
[O_2]	mol%	12
[N_2]	ppm	Balance
Total flow rate	SLPM	5.35
Catalyst length	cm	2
Channel diameter	cm	0.216 for 100 cpsi, 0.150 for 230 cpsi, 0.109 for 400 cpsi

In these experiments, the same catalyst sample was used for all reductants except toluene. For the experiments with toluene, a new catalyst sample of the same composition was used and it was retested with octane to establish a baseline between the two catalyst samples.

It should be noted that experiments were not conducted with pentane, heptane, and nonane as reductants. Experimental data for these hydrocarbons was generated by interpolation from other neighboring hydrocarbon experiments and was used in the model development.

Experimental data for ethanol-SCR were also collected on a pilot-scale reactor, where NO_x conversion and compositions of other species, such as CH_3CHO (acetaldehyde), CH_2O (formaldehyde), HCN (hydrogen cyanide), NH_3 (ammonia), CO, and C_2H_4 (ethylene) were measured as a function of catalyst length at different temperatures, space velocities, and C_1:NO_x ratios using an extractive FTIR analyzer. The pilot test data are not presented in this paper.

3. Development of a HC-SCR microkinetic mechanism on silver

3.1. Literature insights

While proposing the reaction pathways for the HC-SCR mechanism, we have considered a hierarchical approach, where a reaction mechanism for ethanol-SCR is developed first and steps for higher alkane-SCR (hereafter referred to as HC-SCR) are subsequently added. Hydrocarbons are hypothesized to get converted into oxygenates, which drive the SCR reaction [8,7]. Oxygenates have been commonly suggested as surface intermediates. In the proposed HC-SCR mechanism, we have utilized this information by connecting the ethanol and higher alkane pathways via oxygenate (ethoxy) species. As mentioned in Section 1, various research groups have investigated the mechanistic aspects of the SCR process. We have employed some of those critical observations while developing our microkinetic mechanism.

Zuzaniuk et al. investigated the difference in reactivity for the organic-nitrito (RO-N-O) and organic-nitro (R-NO_2) compounds [40]. They found that nitrito compounds mainly yield NO_2, whereas the nitro compounds mainly give rise to NH_3. Yeom et al. suggested that nitrite compounds are important at low temperatures (200 °C), but the nitro compound is significantly formed at higher temperatures (320 °C) [41]. Since formation of NH_3 is consistent with our pilot test data, we believe that the main intermediates are nitro-based rather than nitrito-based.

Cordi and Falconer have studied the oxidation of ethanol on Ag/Al_2O_3 using temperature programmed desorption (TPD) and temperature programmed oxidation (TPO) [42]. Their ethanol-TPD results showed that dehydration to ethylene is the most dominant path. More than 60% of the ethanol dehydrated to ethylene. However, in the presence of oxygen, Ag is more active for dehydrogenation, producing acetaldehyde. Their acetaldehyde-TPD results indicated that acetaldehyde decomposes very slowly to CO, CO_2, and H_2, but it is more reactive in presence of oxygen. Yu et al. studied the mechanism of ethanol-SCR on Ag/Al_2O_3 using in situ diffuse reflectance infrared Fourier transform spectroscopy (DRIFTS) [43]. They observed that ethanol and acetaldehyde show the same activity for NO_x conversion. Based on this, we speculate that acetaldehyde could be a main product of ethanol. Yeom et al. also suggested that ethanol principally reacts with oxygen to form acetaldehyde [41].

Using IR spectroscopy, Usiku et al. found that methanol is less reactive than ethanol for the formation of NCO (isocyanate) species, which is an important intermediate in alcohol-based SCR [44]. This indicated that ethanol-SCR could be more efficient than

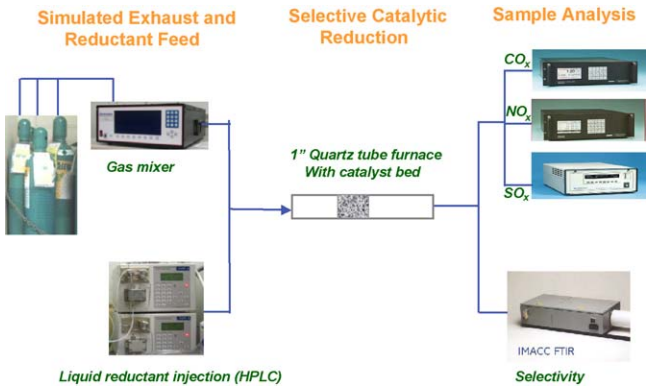

Fig. 1. Schematic of the lab-scale experimental setup.

methanol-SCR. Kameoka et al. found that thermal decomposition of $C_2H_5NO_2$ (nitroethane) is slower than that of CH_3NO_2 (nitromethane) for the formation of NCO species [45]. Since ethanol-SCR is faster than methanol-SCR, this could mean that CH_3NO_2 or similar compounds (CH_2NO_2) could be the main nitro species in ethanol-SCR, rather than $C_2H_5NO_2$.

Using pulse reaction technique and DRIFTS, Kameoka et al. showed that formation of NCO intermediate is enhanced in the presence of Ag compared to Al_2O_3, in the ethanol-SCR system [38]. Using quantum mechanical density functional theory (DFT), Gao and He proposed that thermal decomposition of CH_3NO_2 leads to the formation of NCO intermediate on Ag above 298 K [46]. Their DFT-based vibrational spectra agreed with the experimental vibrational spectra. According to Yeom et al., there is evidence that the aci-anion of nitromethane is an intermediate in the deNO_x (SCR) process on Ag/Al_2O_3 [41]. NH_3 is finally formed by the hydrolysis of NCO ions.

In some recent papers, Burch research group demonstrated the promoting effect of H_2 on the octane-SCR chemistry [16,13]. These papers suggested that H_2 has a direct chemical effect on the reaction mechanism rather than a change in the structure of the active sites. Murzin research group also investigated the SCR mechanism using H_2 as a reductant and proposed that the role of H_2 is to keep the Ag surface reduced [22]. They also found that H_2 by itself is not a good reductant. Our lab-scale experimental data also supports the promoting effect of H_2. This suggests that even though H_2 alone is not sufficient for NO_x reduction, its promoting effect on HC-SCR should be considered while developing the model.

3.2. Reaction pathways

Based on these literature insights, two major pathways are proposed for ethanol consumption on an Ag-based catalyst, as shown in Fig. 2. The first pathway oxidizes ethanol to acetaldehyde, forms the isocyanate intermediate, and eventually produces N-containing compounds such as HCN and NH_3. A competitive pathway is dehydration of ethanol to ethylene followed by subsequent oxidation to CO and CO_2. Both pathways are connected to each other via a variety of intermediates. These pathways are proposed based on the literature insights regarding various intermediates for HC-SCR of NO_x.

Reactions proposed in the ethanol-SCR mechanism constitute the backbone of the HC-SCR mechanism. For every alkane species added to the ethanol-SCR mechanism, the following reactions are included (R stands for alkyl):

$RH + {}^* \leftrightarrow RH^*$	alkane adsorption/desorption
$RH^* + O^* \leftrightarrow RO^* + H^*$	alkoxy formation
$RO^* + OH^* \leftrightarrow R'O^* + C_2H_5O^*$	alkoxy oxidation
$RO^* + H^* \leftrightarrow R^* + OH^*$	alkyl formation
$R^* + OH^* \leftrightarrow R'^* + C_2H_5O^*$	alkyl oxidation

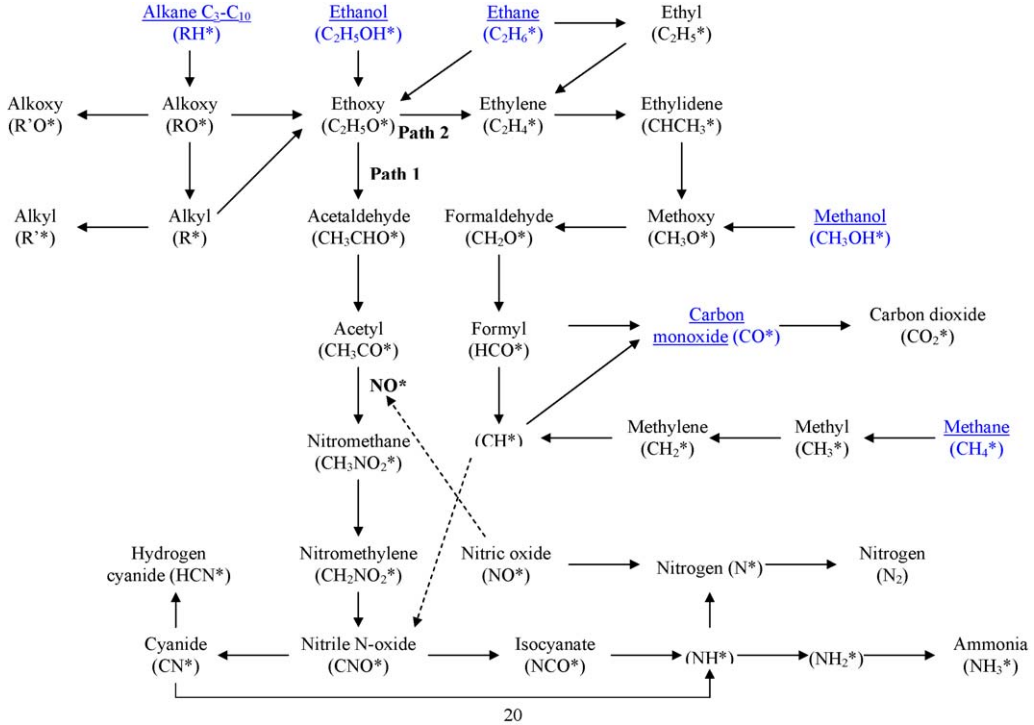

Fig. 2. Schematic of the HC-SCR reaction chemistry. Only selected reactions are shown here. Paths 1 and 2 correspond to SCR and combustion, respectively. Reductant species are underlined.

The ethoxy species can further follow path 1 (SCR) or 2 (oxidation) in Fig. 2. The alkane-SCR chemistry is also schematically shown in Fig. 2. Overall, we have considered a total of 13 reductants (CO, methanol, ethanol, and C_1–C_{10} alkanes) in the HC-SCR mechanism.

As mentioned above, H_2 has a promoting effect on the HC-SCR chemistry. Even though multiple mechanistic opinions have been proposed in the literature, we have incorporated this effect in the microkinetic mechanism via a single reaction given as

$$NO^* + H^* \leftrightarrow N^* + OH^* \qquad H_2\text{-SCR}$$

Once N* is produced via this reaction, it can give rise to increased NO_x conversion. A crucial observation from our experiments is that the H_2 promoting effect is strongest at low temperatures (~300 °C) and weak to none at higher temperatures (375–435 °C). This is possible if the rate of reaction between NO* and H* decreases as a function of temperature. To capture this behavior, an empirical correction is introduced in the form of a negative temperature exponent (β) (where, $rate = AT^{\beta} e^{-E/(RT)}$).

In our lab-scale experiments, we have also investigated the effect of aromatic species (toluene) on the HC-SCR activity. We believe that the aromatic components block the active catalyst surface and inhibit the SCR reaction. This blocking effect is incorporated in the microkinetic mechanism by a single reaction given as

$$C_7H_8 + {}^* \leftrightarrow C_7H_8{}^* \qquad \text{toluene adsorption/desorption}$$

Here, it is assumed that the aromatic species do not participate in any chemical reaction with other surface or gas phase species.

The ethanol-SCR chemistry is fairly extensive (>100 irreversible reactions); however further addition of each alkane results in addition of only 12 reactions. The total number of irreversible reactions after including all HC reductants is only 220 (110 reversible reactions). The mechanism is primary dominated by series reactions rather than parallel reactions and only the sequential steps that are relevant to the species formation/destruction are considered to minimize the number of total reactions. This approach of adding only a few reactions to capture the chemistry of a different additional species is based on the hierarchical microkinetic modeling concept proposed by Vlachos research group [36,29,30].

3.3. Parameter estimation

A surface reaction mechanism requires five types of input parameters: (1) site density, (2) sticking coefficients/pre-exponential factors, (3) temperature exponent, (4) heats of adsorption/activation energies, and (5) coverage dependent parameters. The site density was assumed to be 10^{15} sites/cm^2. All sticking coefficients are taken as unity. The pre-exponential factors are based on transition state theory (TST) order of magnitude estimates [28]. All temperature exponents (β) are zero (except for reaction $NO^* + H^* \leftrightarrow N^* + OH^*$, where the value of β is optimized based on the trend of H_2 effect for various reductants). Heats of adsorption values for some species are taken from surface science experiments and quantum mechanical density functional theory (DFT) calculations in the literature, whereas for the rest of the species, the heats of adsorption values are computed using the semi-empirical Unity Bond Index-Quadratic Exponential Potential (UBI-QEP) method [47–49]. Table 2 compares the heats of adsorption values computed using UBI-QEP and available literature values. Even though the UBI-QEP-based values are in decent agreement with the literature values, there is a significant spread in the literature values, primarily due to different estimation methods or experimental techniques as well as different catalyst supports or planes. UBI-QEP method cannot precisely capture the effects of different supports or operating conditions, whereas DFT

Table 2
Summary of heats of adsorption values based on UBI-QEP estimates, literature experiments, and literature calculations. Units are kcal/mol.

Species	UBI-QEP	Literature experiments	Literature calculations	Interpolated, extrapolated, or tuned value
N	100	<125.2[a]	83–94	–
O	80	76.6–79	73.8–95.2	–
H	52	53	47.9–55.2	–
C	110.3	–	82	–
N_2	8.2	–	11.4[b]	–
O_2	9.5	10–11.5	11.5	–
H_2	4.7	5.5	–	–
NO	17.1[c], 30.5[d]	24.9–25	20.5	–
NO_2	12.7	18	7.2–9.8	-
NH	55.6	–	–	–
NH_2	36.9	–	–	–
NH_3	10.6	11	12.3	–
OH	60.1	65	55.9	–
H_2O	8.5	9.6–14	–	–
CO	13.5	6–6.5	12.5–19	–
CO_2	3.2	9.3	–	–
CH	63.7	–	69.7–97.5	–
CH_2	41.7	–	30–50.9	–
HCO	23.3	–	–	–
CH_2O	10.1	6.2	–	–
CNO	47.6	–	–	–
CN	42	–	–	–
HCN	11.8	–	–	–
NCO	46.9	–	–	–
CH_3CO	23.6	–	–	–
CH_3NO_2	10.4[e]	–	–	–
CH_2NO_2	25.2[c], 34[d]	–	–	–
C_2H_4	6.1	8–10	8.7–14.3	–
$CHCH_3$	60.4	–	33.9	–
CH_3CHO	10.3	9	–	–
CH_3OH	9.5	9.5	–	–
C_2H_5OH	9.4	–	–	–
CH_4	–	–	–	3.5[f]
C_2H_6	–	–	–	5.9[f]
C_3H_8	–	9.5	–	–
C_4H_{10}	–	10.6	–	–
C_5H_{12}	–	–	–	13.1[f]
C_6H_{14}	–	13.9	–	–
C_7H_{16}	–	17	–	–
C_8H_{18}	–	20.9	–	–
C_9H_{20}	–	23.8	–	–
$C_{10}H_{22}$	–	–	–	25.2[f]
CH_3O	37.5	–	44	–
C_2H_5O	37.4	–	–	–
C_3H_7O	36.6	–	–	–
C_4H_9O	36.8	–	–	–
$C_5H_{11}O$	36.8	–	–	–
$C_6H_{13}O$	36.8	–	–	–
$C_7H_{15}O$	36.8	–	–	–
$C_8H_{17}O$	36.8	–	–	–
$C_9H_{19}O$	37.1	–	–	–
$C_{10}H_{21}O$	38.2	–	–	–
CH_3	22.1	–	23.9–29.7	–
C_2H_5	22.7	–	22.7	–
C_3H_7	23.4	–	–	–
C_4H_9	23.5	–	–	–
C_5H_{11}	23.6	–	–	–
C_6H_{13}	23.6	–	–	–
C_7H_{15}	23.6	–	–	–
C_8H_{17}	23.4	–	–	–
C_9H_{19}	23.6	–	–	–
$C_{10}H_{21}$	23.8	–	–	–
C_7H_8	–	–	–	27.1[g]

[a] Computed from N_2 associative desorption energy of 107 kJ/mol by assuming non-activated dissociative adsorption. Therefore, heat of N adsorption is an upper limit.
[b] On Ag/zeolite catalyst.
[c] Medium binding.
[d] Strong binding.
[e] Experimental data on Au and Pt is in the range of 10.5–11 kcal/mol.
[f] Computed from a linear fit of heat of alkane adsorption (Q) vs. carbon number (C_n) (see Fig. 3 and text for additional details). Fit: $Q = 2.4056C_n + 1.1155$ kcal/mol.
[g] Tuned to capture the site blocking effect of toluene (see text for additional details).

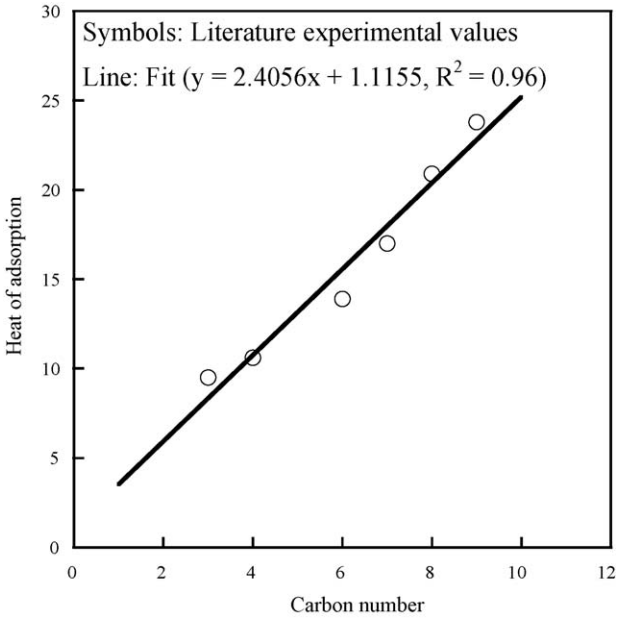

Fig. 3. Linear fit of heat of alkane adsorption vs. carbon number. This fit is used to compute heats of adsorption values for some alkanes (C_1, C_2, C_5, and C_{10}), in absence of experimental data.

values are not available for most of the species that we have considered. Given this large uncertainty, average/intermediate values between theory and experiments are chosen to minimize the error associated with the heats of adsorption. In case of alkanes, a linear fit is used based on the available heats of adsorption values, as shown in Fig. 3. Using the selected heats of adsorption values as inputs to the UBI-QEP methodology [47], we then compute the activation energies of all surface reactions.

3.4. Parameter tuning

Given the uncertainty in parameter estimation for some species due to different estimation methods and unavailability of data in certain cases, some parameter tuning is required to quantitatively match the SCR experimental data. We have tuned a few pre-exponential factors, activation energies, and introduced O*-coverage dependence in some selected reactions to match our pilot test ethanol-SCR data.

The HC-SCR mechanism is tuned based on our lab-scale experimental data. It is observed that the activation energies of alkoxy/alkane formation steps ($RH^* + O^* \leftrightarrow RO^* + H^*$) are the most important parameters in controlling the overall conversion response. Shustorovich and Sellers have used a bond index of 0.5 in calculating the activation energies using UBI-QEP method [47]. The bond indices of the alkoxy/alkane formation steps are tuned in the range of ~0.45–0.6 to capture the experimental SCR conversion with each alkane. Such bond index modification has been proposed previously for CO oxidation [50] and methane oxidation [29] on Pt. It should be noted that propylene and isobutylene reductants were approximated as propane and butane, respectively, while tuning the parameters.

As mentioned above, the value of β for reaction $NO^* + H^* \leftrightarrow N^* + OH^*$ is optimized to −0.5 based on the trend of H_2 effect for various reductants. Heat of adsorption of toluene is adjusted such that it captures the blocking effect on HC-SCR at one selected temperature.

Based on the perspective of purely theoretical mechanism development, e.g., using only quantum mechanical DFT or TST, such parameter tuning may seem inconsistent. However, it is important to note that this microkinetic mechanism is developed for a fairly large reaction system (13 different reductants, H_2 effect, and aromatic effect) by considering only 220 (110 reversible) elementary-like reactions, thus maintaining the computational feasibility of its application. Some parameter tuning is justified to capture such large number of effects in a single mechanism and is a common practice in the development of microkinetic models that try to account for a variety of experimental data sets.

4. Performance of the HC-SCR mechanism

Each monolith channel in the lab-scale experiments is modeled as a plug flow reactor (PFR) using Reaction Design (Chemkin interface) version 4.1 [51]. The governing equations could be found in the Reaction Design software documentation.

4.1. Baseline performance

Fig. 4 shows the performance of the HC-SCR mechanism against our experimental data. As mentioned above, the bond indices of alkoxy/alkane formation steps ($RH^* + O^* \leftrightarrow RO^* + H^*$) are tuned to match the experimental NO_x conversion at 375 °C only. Data at the two other temperatures (305 and 435 °C) are predicted using the mechanism. A critical point to observe here is that the NO_x conversion decreases at higher temperatures (435 °C) compared to that at 375 °C. Broadly, the NO_x reduction process is a combination of two competing paths, viz., the SCR path and combustion path. At high temperatures, contribution of the combustion path starts increasing, resulting in a decrease in the observed NO_x conversion. Since the HC-SCR mechanism also consists of SCR and combustion paths (see Fig. 2), it is able to predict the decrease in NO_x conversion at high temperatures. Overall performance of the mechanism is also summarized in Fig. 5, where the parity plot compares the experimental and calculated NO_x conversion values for all reductants at three temperatures (305, 375, and 435 °C). Good agreement is observed between the mechanism predictions and experimental data with $R^2 = 0.94$. It should be noted that conversion values at 305 °C are low (~5%) and therefore, are

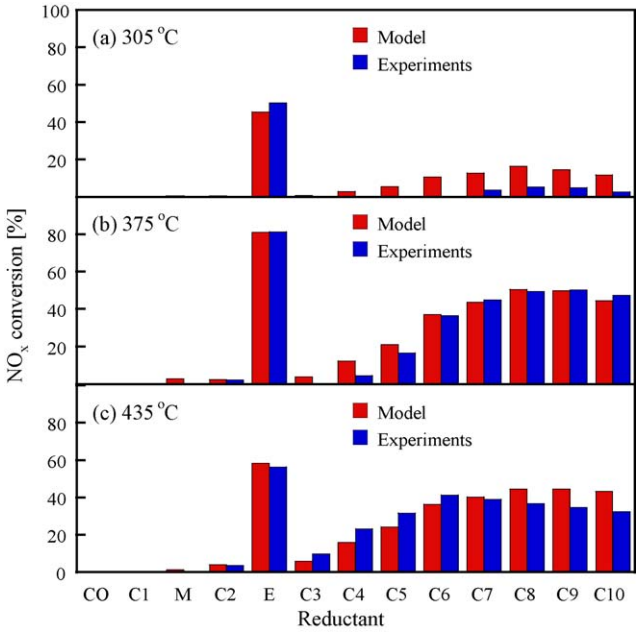

Fig. 4. Comparison of model predictions using the HC-SCR mechanism for 13 different reductants and experimental data, at three temperatures. M and E stand for methanol and ethanol, respectively. Operating conditions are given in Table 1. Monolith cell density is 230 cpsi. No H_2 or toluene in feed.

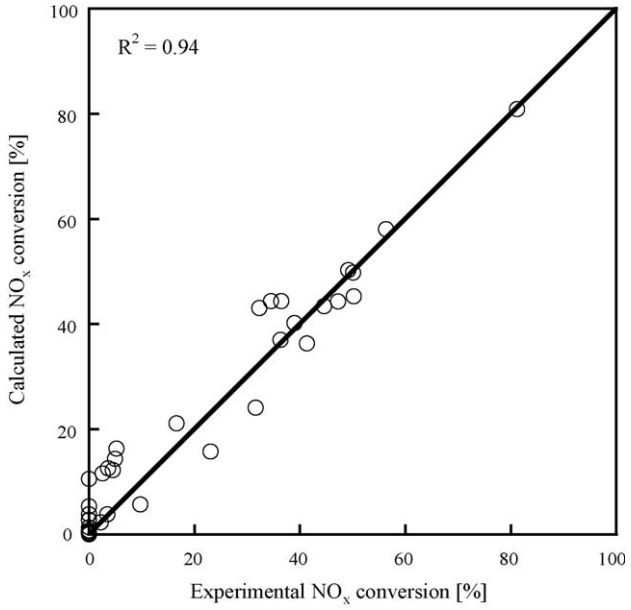

Fig. 5. Parity plot showing the collective performance of the HC-SCR mechanism against experimental data for all 13 reductants at three temperatures. The data are same as in Fig. 4.

associated with a larger relative uncertainty due to variation in reactor operation, as compared to higher temperatures. In general, the model predictions are within absolute 5–10% of the experimental data, even at low temperature. While conducting these simulations, the catalyst area per unit length (πd = 0.4708 cm) is not tuned; it is computed from the channel diameter corresponding to a 230 cpsi monolith. Furthermore, even though the experimental NO_x conversion values for CO, methane, methanol, and ethane are very low, it should be noted that the model predictions are consistent with these values.

To illustrate the primary gas phase species forming in the reactor, axial profiles of mole fractions are plotted in Fig. 6. Primary gaseous products of the HC-NO_x reaction are H_2O, ethylene, CO, and CO_2. Some minor products such as hydrogen cyanide, formaldehyde, acetaldehyde, and NH_3 are also observed. This is consistent with our FTIR-based observations on an ethanol-SCR system. Significant amount of oxygen is consumed compared to the hydrocarbon (in this case, octane) and NO, which emphasizes that SCR reactions have to compete the combustion reactions in presence of abundant oxygen and therefore, C_1:$NO_x > 1$ is typically needed for effective NO_x removal. Similarly, Fig. 7 shows the most abundant reaction intermediates on the catalyst surface. The surface is largely covered by OH* and O*, as expected, given the large amount of oxygen fed at the inlet (12%). Therefore, reactions of other species with OH* and O* should be important and are considered in the reaction mechanism. Some of the other surface intermediates include NO* and alkoxy (in this case, octoxy) species.

4.2. Effect of hydrogen

Next, we show the performance of the HC-SCR mechanism for the same 13 reductants, in presence of 1000 ppm hydrogen at inlet. Fig. 8 shows the promoting effect for ethanol-SCR and octane-SCR by comparing data in absence and presence of hydrogen. Fig. 9 shows the HC-SCR mechanism predictions for all 13 reductants in presence of hydrogen, and Fig. 10 shows the parity plot. The SCR promoting effect at low temperature is reasonably well captured by the mechanism (R^2 = 0.78). At higher temperature, the H_2 promoting effect is reduced, probably due to oxidation of hydrogen. Even though our mechanism includes oxidation

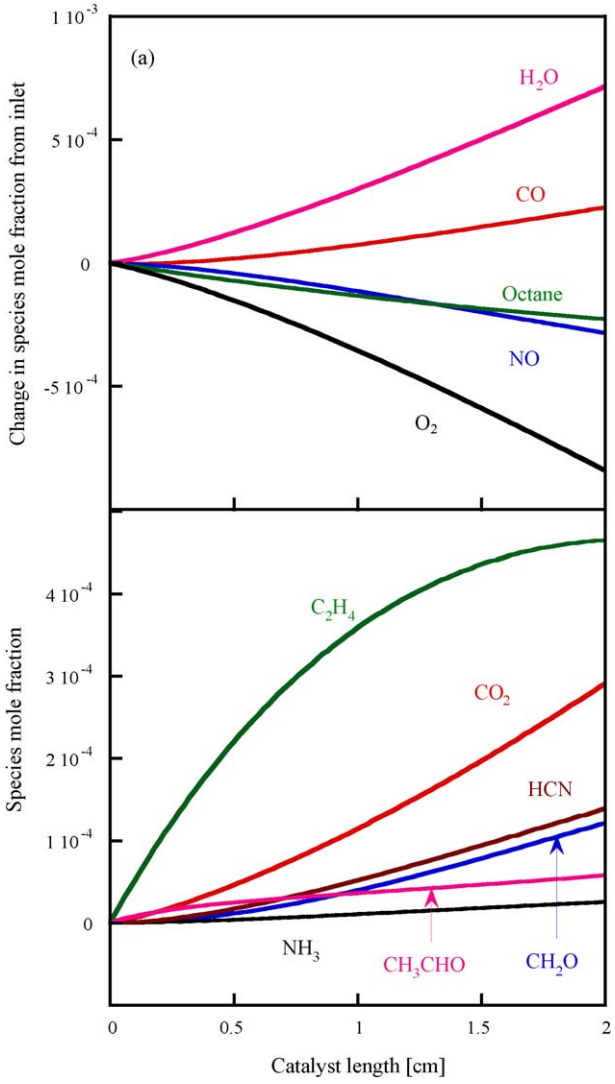

Fig. 6. Profiles of calculated axial mole fractions for selected gas phase species in octane-SCR, corresponding to operating conditions in Fig. 4 and at a temperature of 375 °C.

reactions for hydrogen, it does not fully capture the reduced promoting effect at high temperature through those reactions alone. Hence, we have chosen to introduce a correction factor in terms of temperature exponent (β). Only one temperature exponent β (for NO* + H* ↔ N* + OH*) is adjusted to −0.5 in order to capture the promoting effect of hydrogen at low temperature. Due to the negative value of β, the model predicted rate of reaction between NO* and H* decreases at higher temperatures. The adjustment in β has no effect on the predictions of the HC-SCR mechanism without hydrogen at inlet. Overall R^2 is 0.87 if data with and without hydrogen is combined (not shown). From the profiles of axial mole fractions and coverages in Fig. 11, it is clear that hydrogen is consumed at the catalyst inlet, mostly via combustion and some H_2-SCR. High coverage of OH* in the inlet portion of the catalyst is a result of NO* + H* ↔ N* + OH* reaction. At higher temperatures, this effect is not observed due to negative β.

4.3. Effect of toluene

Presence of aromatic species in the reductant stream can seriously hinder the progress of the SCR reaction. This is especially

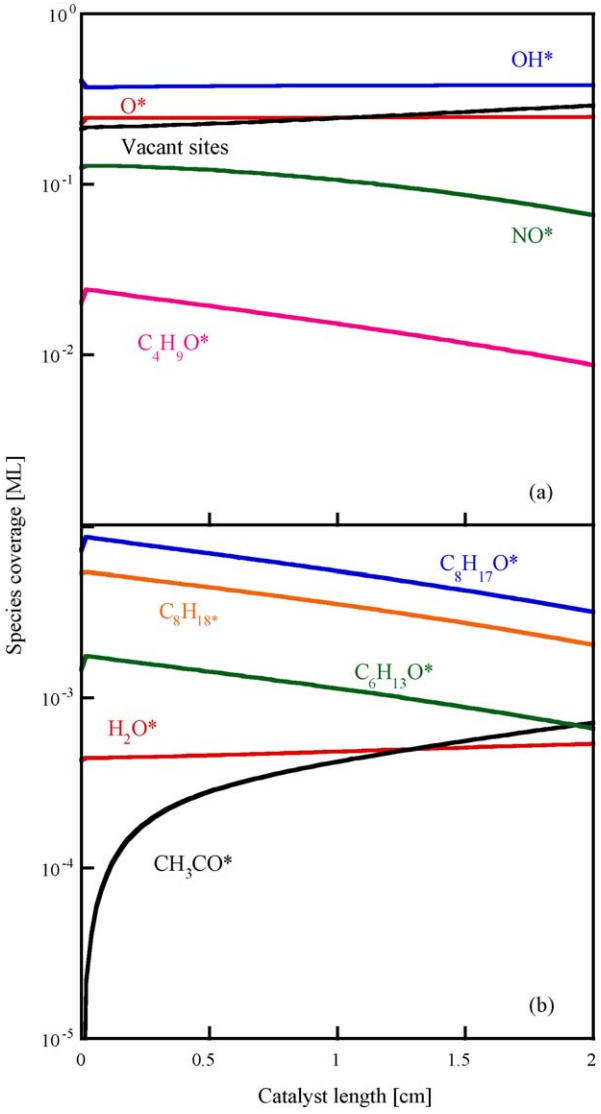

Fig. 7. Profiles of coverages (ML stands for monolayer) for selected surface species in octane-SCR, corresponding to operating conditions in Fig. 4 and at a temperature of 375 °C.

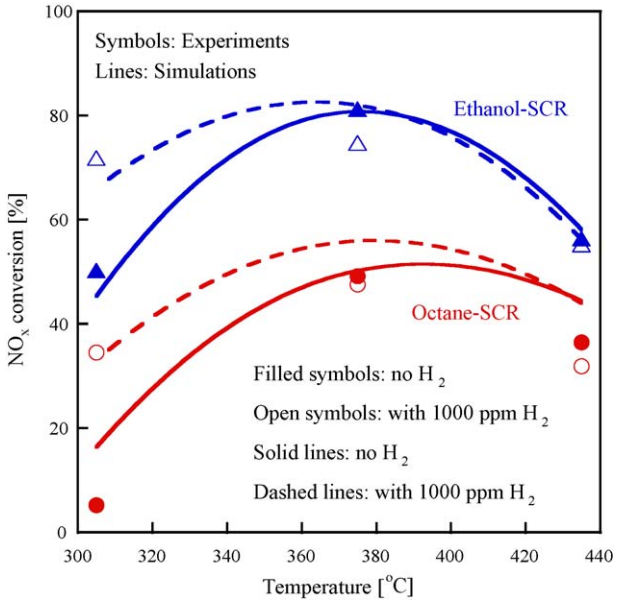

Fig. 8. Promoting effect of 1000 ppm hydrogen on ethanol-SCR and octane-SCR. Operating conditions are given in Table 1. Monolith cell density is 230 cpsi. No toluene in feed.

true for diesel-based SCR. As discussed earlier, the inhibiting effect of aromatic species is incorporated into the mechanism by adding the reaction of toluene adsorption/desorption.

It should be noted that the same catalyst composition with different washcoat loading (different activity) was used in these experiments, as mentioned in Section 2. This change is taken into account by adjusting the value of active catalyst area per unit length in the Chemkin simulations, to match the experimentally observed conversion with octane reductant at 375 °C. No other parameters were adjusted.

Experiments were conducted for three cases: (1) pure octane with C_1:NO_x = 5:1, 2) octane + toluene with total C_1:NO_x = 5:1 (equal C_1:NO_x = 2.5:1 for octane and toluene), and (3) octane + toluene with total C_1:NO_x = 10:1 (equal C_1:NO_x = 5:1 for octane and toluene). As expected, presence of toluene decreases the SCR performance, both when it replaces a portion of octane and when it is added to octane. Experimental data and the predictions of the HC-SCR mechanism are shown in Fig. 12. The HC-SCR mechanism fairly captures the inhibiting effect for these cases when a single parameter (heat of toluene adsorption) is adjusted to match experimental observations at 375 °C. Coverage profiles along the catalyst length in Fig. 13 clearly show that toluene blocks a significant amount of catalyst sites, resulting in a decrease in the NO_x conversion. Fig. 12 also shows the combination of toluene's inhibiting effect and hydrogen's promoting effect. The HC-SCR mechanism is able to correctly predict the trends.

An interesting observation from Fig. 12 is that the inhibiting effect of toluene is reduced with an increase in temperature. We believe that at high temperature, toluene will either desorb from the surface or get oxidized. This will result in a less site-inhibiting effect, which could explain this trend. In the microkinetic model, even though we do not consider any toluene oxidation reactions, this effect is accounted for through the toluene adsorption/desorption reaction. As the temperature increases, rate of toluene desorption increases, and the surface coverage of toluene decreases (0.44 at 305 °C, 0.34 at 375 °C, and 0.16 at 435 °C).

4.4. Parametric trends

With the aid of the developed HC-SCR mechanism, different parametric effects can be investigated. Since experimental data is not available to compare with the predictions, these predictions should only be considered qualitative. The effect of temperature has already been discussed in Figs. 4, 8, 9 and 12. Fig. 14 shows the effect of space velocity, C_1:NO_x ratio, and monolith cell density on NO_x conversion. Trends in Fig. 14 are consistent with the general expectations. NO_x conversion decreases with increasing space velocity (decreasing residence time), higher C_1:NO_x (increased reductant) increases NO_x conversion, and higher cell density (more catalyst area per unit volume of reactor due to smaller channel diameter) is beneficial for improving NO_x conversion.

5. Assumptions/limitations of the HC-SCR mechanism

With optimization of only a few kinetic parameters, the HC-SCR mechanism is able to predict data for 13 different reductants; it quantitatively captures the effect of temperature, promoting effect of hydrogen, inhibiting effect of toluene (aromatic species), and it predicts the correct trends with respect to additional parameters such as space velocity, inlet composition (C_1:NO_x ratio), and monolith cell density. To our knowledge, this is the first comprehensive microkinetic model developed for HC-SCR. None-

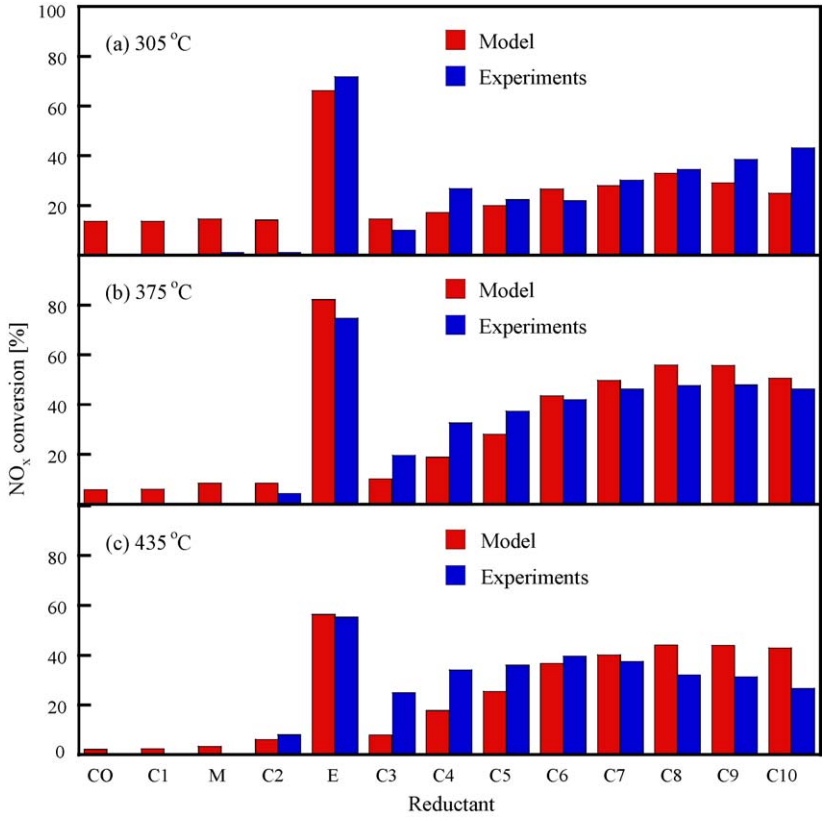

Fig. 9. Comparison of model predictions using the HC-SCR mechanism for 13 different reductants and experimental data, at three temperatures, in presence of 1000 ppm H_2 in feed. M and E stand for methanol and ethanol, respectively. Operating conditions are same as in Fig. 8.

theless; it is imperative to acknowledge the assumptions and limitations related to the development and performance of the HC-SCR mechanism:

- The HC-SCR mechanism is not completely thermodynamically consistent. This issue arises due to the adjustment of some pre-exponential factors and activation energies to capture the experimental data. This could be an important issue for equilibrium limited reactions, such as $NO \leftrightarrow NO_2$. A solution to partially fix the thermodynamic inconsistency issue would be to treat the heats of surface reactions as linear combinations of heats of adsorption [27]. If the activation energies are computed using a consistent method such as UBI-QEP or DFT, the mechanism should be enthalpically consistent. Similarly, the entropies of reactions must be considered as linear combinations of the entropies of adsorption [27], which should ensure entropic consistency on the mechanism level. Since entropies of adsorption are generally not available from experiments or cannot be computed from methods such as UBI-QEP, the two possible solutions are to estimate the pre-exponential factors using DFT-TST or optimization to minimize the net entropic error [27].
- Literature data for heats of adsorption show a lot of uncertainty/spread. The primary source of variation arises from catalyst structure (single crystal surfaces vs. polycrystalline supported catalysts). Another important source is method of parameter estimation (experiments vs. cluster calculations vs. periodic slab calculations). Furthermore, even though UBI-QEP method is extremely useful for such computations, its applicability for larger molecules cannot be verified in the absence of reliable experimental or theoretical data.
- Axial profiles of various species were taken into account while developing the ethanol-SCR mechanism. However, while developing the HC-SCR mechanism, only NO_x conversion is taken into consideration as the experimental response. Given the complexity of the reaction mechanism and the possibility of forming many products, it is important to consider additional experimental responses, such as species mole fractions. Experimental identification of the surface intermediates at different catalyst

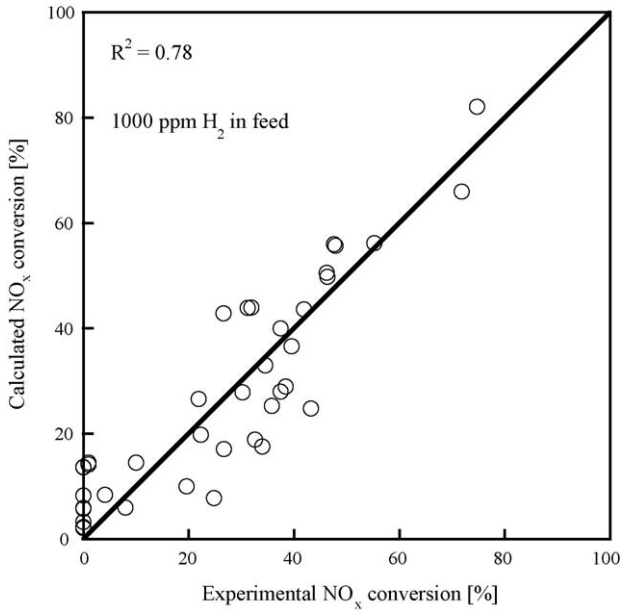

Fig. 10. Parity plot showing the collective performance of the HC-SCR mechanism against experimental data for all 13 reductants, at three temperatures, in presence of 1000 ppm H_2 in feed. The data are same as in Fig. 9.

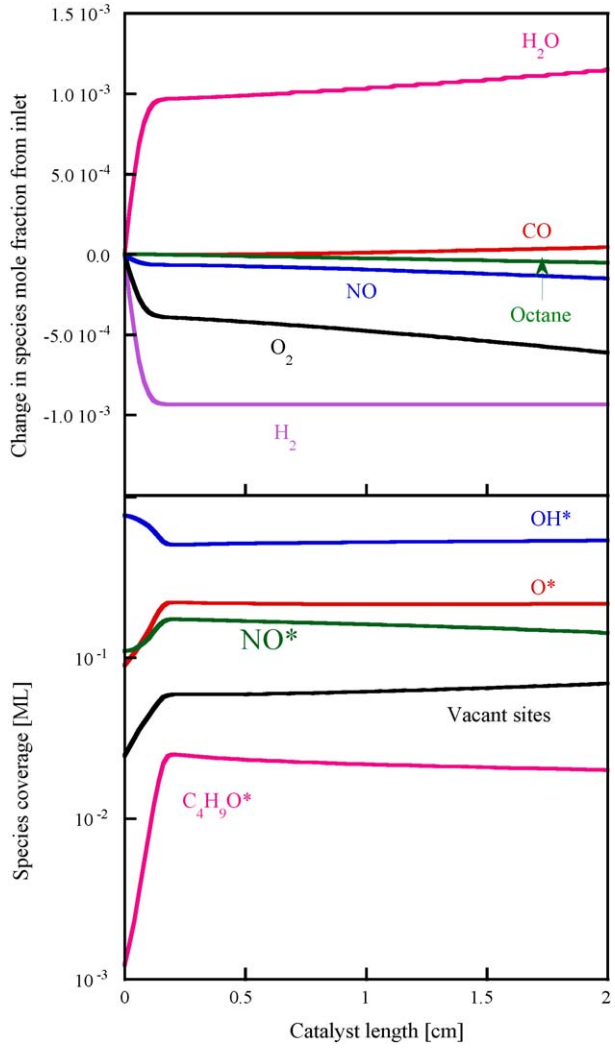

Fig. 11. Profiles of axial mole fractions for selected gas phase species and coverages (ML stands for monolayer) for selected surface species in octane-SCR, corresponding to operating conditions in Fig. 9 and at a temperature of 305 °C, in presence of 1000 ppm H_2 in feed.

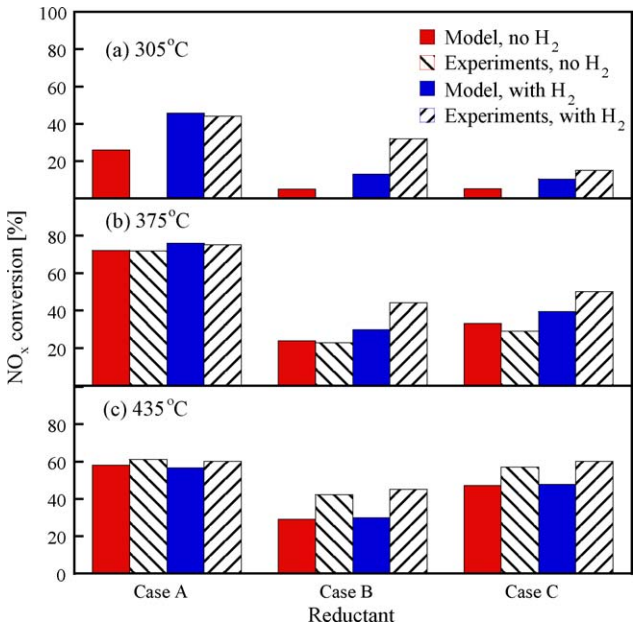

Fig. 12. Comparison of model predictions using the HC-SCR mechanism and experimental data, showing the effect of aromatic species (toluene). Case A: pure octane with C_1:NO_x = 5:1, case B: octane + toluene with total C_1:NO_x = 5:1 (equal C_1:NO_x = 2.5:1 for octane and toluene), and case C: octane + toluene with total C_1:NO_x = 10:1 (equal C_1:NO_x = 5:1 for octane and toluene). Effect of 1000 ppm H_2 in feed is also shown. Operating conditions are given in Table 1. Monolith cell density is 230 cpsi.

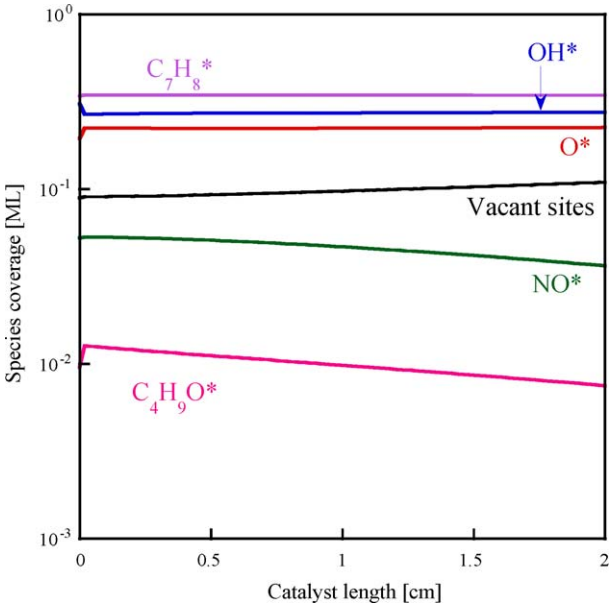

Fig. 13. Profiles of coverages (ML stands for monolayer) for selected surface species in octane-SCR, corresponding to operating conditions in case C of Fig. 12 and at a temperature of 375 °C, in presence of toluene. No H_2 in feed.

locations could also be beneficial for additional verification of the mechanism's predictive capabilities.

- Alkenes and isomers of alkanes are approximated as alkanes in the HC-SCR mechanism. Even though the chemistry of alkenes and alkanes is expected to be qualitatively similar, the nature of intermediate species might be different. Additional experimental information is needed to resolve this issue.
- The promoting effect of hydrogen and inhibiting effect of toluene are captured by adjustment of a single kinetic parameter in each case. The first modification essentially results in H_2-SCR at the front of the catalyst and the possibility of reduction of silver surface is not considered in this mechanism. The second modification helps in capturing the blocking effect of toluene, however it does not consider any chemical reactions with other species or decomposition to coke. Additional experimental data is needed to quantitatively verify the mechanism performance.
- Effect of gas phase chemistry is not taken into account due to unavailability of a suitable gas phase elementary reaction mechanism.
- A time scale analysis for convection, axial diffusion, and radial diffusion indicates that the convection rate is much faster than the axial diffusion rate, confirming the validity of the PFR model. Rates of convection and radial diffusion are comparable, which indicates that under those conditions, external mass transfer limitations could be equally important as the kinetics. Given the complexity of the reaction mechanism, we have not accounted for the external mass transfer limitations in this work, and therefore some rate parameters would be affected by external mass transfer limitations.

As more experimental data becomes available, we aim to remove most of these assumptions/limitations in the future work.

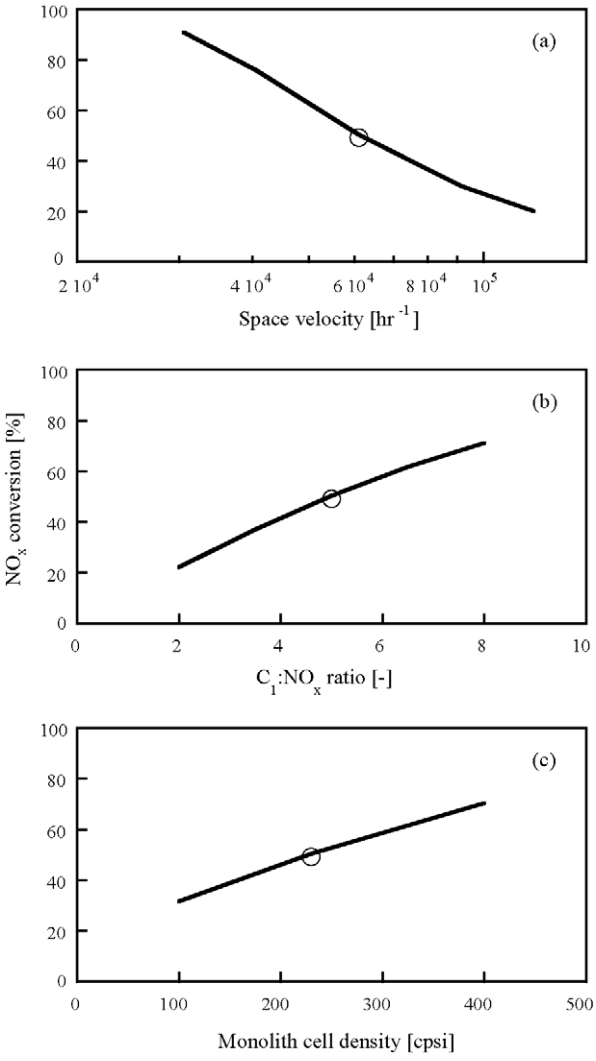

Fig. 14. Predictions of qualitative trends using the HC-SCR mechanism. Effects of space velocity, C_1:NO_x ratio, and monolith cell density are studied for octane-SCR. Operating conditions are given in Table 1. Temperature = 375 °C. No H_2 or toluene in feed. (a) Monolith cell density = 230 cpsi and C_1:NO_x = 5:1, (b) monolith cell density = 230 cpsi and space velocity = 61,000 h^{-1}, and (c) C_1:NO_x = 5:1 and space velocity = 61,000 h^{-1}. Data point represented by a circle indicates the available experimental point under nominal conditions.

6. Conclusions

A novel comprehensive microkinetic mechanism is developed for HC-SCR, using literature insights regarding reaction pathways, literature data of heats of adsorption, semi-empirical UBI-QEP estimates, and parameter optimization based on pilot-scale and lab-scale experiments. To our knowledge, this is the first elementary step mechanism that can predict SCR performance for a total of 13 reductants (CO, methanol, ethanol, and C_1–C_{10} alkanes) at different temperatures. Promoting effect of hydrogen and site-blocking effect of aromatic species (toluene) are also captured by this mechanism, via minimum parameter tuning. Various assumptions and limitations in the mechanism development and performance are acknowledged, most of which need additional experimental data for further improvement.

Acknowledgments

The authors would like to thank Teresa Grocela-Rocha, Roland Sedziol, and Narendra Joshi for their support of this project.

References

[1] M.V. Twigg, Appl. Catal. B 70 (2007) 2.
[2] U.G. Alkemade, B. Schumann, Solid State Ionics 177 (2006) 2291.
[3] P. Sazama, L. Capek, H. Drobna, Z. Sobalik, J. Dedecek, K. Arve, B. Wichterlova, J. Catal. 232 (2005) 302.
[4] M.H. Kim, I.-S. Nam, Catalysis 18 (2005) 116.
[5] R. Burch, Catal. Rev. 46 (2004) 271.
[6] V.A. Sadykov, V.V. Lunin, V.A. Matyshak, E.A. Paukshtis, A.Y. Rozovskii, N.N. Bulgakov, J.R.H. Ross, Kinet. Catal. 44 (2003) 379.
[7] A. Satsuma, K.-I. Shimizu, Prog. Energy Combust. Sci. 29 (2003) 71.
[8] R. Burch, J.P. Breen, F.C. Meunier, Appl. Catal. B: Environ. 39 (2002) 283.
[9] P. Forzatti, Appl. Catal. A 222 (2001) 221.
[10] Y. Traa, B. Burger, J. Weitkamp, Micropor. Mesopor. Mater. 30 (1999) 3.
[11] G. Busca, L. Lietti, G. Ramis, F. Berti, Appl. Catal. B 18 (1998) 1.
[12] V.I. Parvulescu, P. Grange, B. Delmon, Catal. Today 46 (1998) 233.
[13] J.P. Breen, R. Burch, C. Hardacre, C.J. Hill, C. Rioche, J. Catal. 246 (2007) 1.
[14] J.P. Breen, R. Burch, C. Hardacre, C.J. Hill, B. Krutzsch, B. Bandl-Konrad, E. Jobson, L. Cider, P.G. Blakeman, L.J. Peace, M.V. Twigg, M. Preis, M. Gottschling, Appl. Catal. B 70 (2007) 36.
[15] J.P. Breen, R. Burch, Top. Catal. 39 (2006) 53.
[16] J.P. Breen, R. Burch, C. Hardacre, C.J. Hill, J. Phys. Chem. B 109 (2005) 4805.
[17] R. Burch, P. Fornasiero, T.C. Watling, J. Catal. 176 (1998) 204.
[18] H. Backman, K. Arve, F. Klingstedt, D.Y. Murzin, Appl. Catal. A 304 (2006) 86.
[19] K. Arve, H. Backman, F. Klingstedt, K. Eranen, D.Y. Murzin, Appl. Catal. A 303 (2006) 96.
[20] K. Arve, F. Klingstedt, K. Eranen, J. Warna, L.-E. Lindfors, D.Y. Murzin, Chem. Eng. J. 107 (2005) 215.
[21] K. Arve, E.A. Popov, F. Klingstedt, K. Eranen, L.-E. Lindfors, J. Eloranta, D.Y. Murzin, Catal. Today 100 (2005) 229.
[22] H. Backman, J. Jensen, F. Klingstedt, T. Salmi, D.Y. Murzin, Appl. Catal. A 294 (2005) 49.
[23] K. Eranen, F. Klingstedt, K. Arve, L.-E. Lindfors, D.Y. Murzin, J. Catal. 227 (2004) 328.
[24] K. Arve, E.A. Popov, M. Ronnholm, F. Klingstedt, J. Eloranta, K. Eranen, D.Y. Murzin, Chem. Eng. Sci. 59 (2004) 5277.
[25] K. Arve, L. Capek, F. Klingstedt, K. Eranen, L.-E. Lindfors, D.Y. Murzin, J. Dedecek, Z. Sobalik, B. Wichterlova, Top. Catal. 30/31 (2004) 91.
[26] K. Eranen, L.-E. Lindfors, F. Klingstedt, D.Y. Murzin, J. Catal. 219 (2003) 25.
[27] A.B. Mhadeshwar, H. Wang, D.G. Vlachos, J. Phys. Chem. B 107 (2003) 12721.
[28] J.A. Dumesic, D.F. Rudd, L.M. Aparicio, J.E. Rekoske, A.A. Trevino, The Microkinetics of Heterogeneous Catalysis, American Chemical Society, Washington, DC, 1993 .
[29] A.B. Mhadeshwar, D.G. Vlachos, Ind. Eng. Chem. Res, 46 (2007) 5310.
[30] A.B. Mhadeshwar, D.G. Vlachos, J. Catal. 109 (2005) 16819.
[31] S.R. Deshmukh, A.B. Mhadeshwar, D.G. Vlachos, Ind. Eng. Chem. Res. 43 (2004) 86.
[32] R. Quiceno, J. Perez-Ramirez, J. Warnatz, O. Deutschmann, Appl. Catal. A 303 (2006) 166.
[33] E. Hecht, G.K. Gupta, H. Zhu, A.M. Dean, R.J. Kee, R. Maier, O. Deutschmann, Appl. Catal. A 295 (2005) 40.
[34] D.K. Zerkle, M.D. Allendorf, M. Wolf, O. Deutschmann, J. Catal. 196 (2000) 18.
[35] F. Donsi, K.A. Williams, L.D. Schmidt, Ind. Eng. Chem. Res. 44 (2005) 3453.
[36] D.G. Vlachos, A.B. Mhadeshwar, N.S. Kaisare, Comp. Chem. Eng. 30 (2006) 12.
[37] K. Eranen, L.-E. Lindfors, A. Niemi, P. Elfving, L. Cider, SAE Paper 2000-01-2813 (2000).
[38] S. Kameoka, T. Chafik, Y. Ukisu, T. Miyadera, Catal. Lett. 55 (1998) 211.
[39] H. He, Y. Yu, Catal. Today 100 (2005) 37.
[40] V. Zuzaniuk, F.C. Meunier, J.R.H. Ross, J. Catal. 202 (2001) 340.
[41] Y.H. Yeom, M. Li, W.M.H. Sachtler, E. Weitz, J. Catal. 238 (2006) 100.
[42] E.M. Cordi, J.L. Falconer, Appl. Catal. A 151 (1997) 179.
[43] Y. Yu, H. He, Q. Feng, H. Gao, X. Yang, Appl. Catal. B 49 (2004) 159.
[44] Y. Usiku, T. Miyadera, A. Abe, K. Yoshida, Catal. Lett. 39 (1996) 265.
[45] S. Kameoka, T. Chafik, Y. Usiku, T. Miyadera, Catal. Lett. 51 (1998) 11.
[46] H. Gao, H. He, Spectrochim. Acta Part A 61 (2005) 1233.
[47] E. Shustorovich, H. Sellers, Surf. Sci. Rep. 31 (1998) 1.
[48] E. Shustorovich, Adv. Catal. 37 (1990) 101.
[49] E.M. Shustorovich, A.V. Zeigarnik, Russ. J. Phys. Chem. 80 (2006) 4.
[50] A.B. Mhadeshwar, D.G. Vlachos, Combust. Flame 142 (2005) 289.
[51] R.J. Kee, et al., CHEMKIN release 4. 1, Reaction Design, San Diego, CA, 2006, Link: http://www.reactiondesign.com/products/open/chemkin.html.